Micro-Doppler Based Target Detection and Feature Extraction in Indoor and Outdoor Environments

Thayananthan Thayaparan, LJubiša Stanković, Igor Djurović

Abstract— **In many cases, a target or a structure on a target may have micro-motions, such as vibrations or rotations. Micro-motions of structures on a target may introduce frequency modulation on the returned radar signal and generate sidebands on the Doppler frequency shift of the target's body. The modulation due to micro-motion is called the micro-Doppler (m-D) phenomenon. In this paper, we present an effective quadratic time-frequency S-method based approach in conjunction with the Viterbi algorithm to extract m-D features. For target recognition applications, mainly those in military surveillance and reconnaissance operations, micro-Doppler features have to be extracted quickly so that they can be used for real-time target identification. The S-method is computationally simple, requiring only slight modifications to the existing Fourier transform-based algorithm. The effectiveness of the S-method in extracting m-D features is demonstrated through the application to indoor and outdoor experimental data sets such as rotating fan and human gait. The Viterbi algorithm for the instantaneous frequency estimation is used to enhance the weak human micro-Doppler features in relatively high noise environments. As such, this paper contributes additional experimental micro-Doppler data and analysis, which should help in developing a better picture of the human gait micro-Doppler research and its applications to indoor and outdoor imaging and automatic gait recognition systems.**

I. Introduction

The ongoing war on terror is quickly becoming asymmetric in nature wherein the old rules of conflict are no longer applicable. The adversary is usually dispersed and attacks come from non-conventional theaters, such as the urban and littoral zones where detection of the well-concealed adversary is impossible by conventional means. Adversaries or criminals hide within and behind building walls and dense foliage making it impossible to detect them by optical means. The only technology that has a reasonable chance of success is microwave radar, which has the ability to penetrate building wall materials, such as concrete, brick, plaster, cloths, and dense foliage.

Journal of The Franklin Institute, Vol. 345, No. 6, Sept. 2008.

There is continuing interest in being able to detect illegal activity behind opaque walls [1], [2], [3]. Radar signals reflected from individual humans contain biometric information related to periodic contraction of a heart, blood vessels, lungs, other fluctuations of the skin in the process of breathing and heart beating [1]. These processes are cyclical and range in frequency from 0.8 to 2.5 Hz for heartbeat and 0.2-0.5 Hz for breathing [1]. Such micro-Doppler (m-D) signals are concealed within other naturally varying signals making detection extremely difficult.

Obtaining radar signatures of humans is another important application of m-D. The human walking gait is a complex motion behavior that comprises different movements of individual body parts. Recently, the development of automatic radar gait recognition technology has grown. Because radar gait recognition technology is so new, researchers are assessing its uniqueness and methods by which it can be evaluated. Various computer vision and ultrasound techniques have been developed to measure gait parameters [4]-[10]. However, real-time automatic gait recognition radar systems have recently been recognized as advantageous solutions for detecting, classifying and identifying human targets from stand-off distances under conditions of multipath, clutter, and foliage obstruction in all light and weather conditions. Radar has certain advantages over electro-optical (EO) systems and video cam-

eras in that it can penetrate clothes, does not require light, and operates in fog and other low-visibility weather conditions. Several research labs and universities have been involved in radar-based gait recognition technology for the past years; nevertheless, more fundamental research is still needed in this area. The radar sends out a signal and then measures the echo that contains rich information about the various parts of the moving human body. Body parts cause different shifts since they are moving with various velocities. In this case, the micro-Doppler refers to Doppler scattering returns produced by non-rigid human body motion. Micro-Doppler gives rise to many detailed radar image features in addition to those associated with bulk human body motion. For example, a walking man with swinging arms may induce frequency modulation (FM) of the returned signal and generate sidebands about the body Doppler. In this paper, we develop the preliminary groundwork for this challenging field of research.

It is reasonable to expect that the m-D features representing the micro-motions such as swinging arms of a human can be extracted from the returned signal, much in the same way as properties are extracted from radar returns of targets undergoing only translational motion. Since different humans can have different micro-motions, every human would have its own "m-D signature", making it possible to distinguish and identify humans under consideration based on the additional information provided by the m-D features. Hence, an effective method is needed for extracting m-D features in order to fully exploit the additional and unique information they provide.

Traditional techniques, such as Fourier analysis or the sliding window FT (short time Fourier transform - STFT), lack the required resolution for extracting and processing these unique m-D features. Therefore, high-resolution linear and quadratic time-frequency (TF) analysis techniques are recently employed for extracting m-D features [11]-[21]. Several papers have been written about the ways to deal with the m-D effect. The wavelet analysis of helicopter and human data, along with the TF representation based imaging system, is presented in [14]-[16]. Details on the m-D effect physics, with some typical examples, are given in [17]-[18]. A method for the separation of the m-D effect from the radar image, based on the chirplet transform, is proposed in [19]. Both wavelet-based and chirplet based procedures are used in [20] to extract the m-D features such as the rotating frequency of the antenna from SAR data. Recently, two techniques for the separation of the target rigid body from m-D parts have been proposed in [21]. The first approach is based on order statistics of the spectrogram samples. The second approach is based on the Radon transform processing of obtained radar signals. The analysis of the TF representations application in radar target identification is presented in [22]. The reduced interference distributions from the Cohen class are applied as a tool for the target identification. A technique for the m-D effect estimation from the reflected signal, based on the TF signatures and decomposition of basis functions, is presented in [23]. This technique can be used for m-D effect signals that can be represented as sinusoidal FM signals. The goal of this paper is to find an improved method, which gives enhanced resolution and suppresses most of the cross-terms in relatively high noise environments.

Micro-Doppler features have great potential for use in automatic target classification algorithms. Although there have been studies of m-D effects in radar in the past few years [11]-[21], there are only a few experimental trials performed so far that are specifically dedicated to human m-D research. The experimental trails used in this paper can be considered as precursors to the more advanced through-wall radar imaging applications. As such, this paper contributes additional experimental m-D data and analysis, which should help in developing a better picture of the human m-D research and its applications to indoor and outdoor radar imaging and automatic gait recognition system.

In this paper, we apply the S-method (SM) based approach, which appears to have great promise to recognize the m-D features such as rotating fan, human gait in indoor and outdoor environments. The SM is also numeri-

cally very simple and requires just a few more operations than the standard FT based algorithm. This technique can improve a radar image with simple postprocessing of the standard radar image. In addition, signal oversampling is avoided while spurious interferences common for some other bilinear TF representations are significantly reduced or removed. Since the m-D signature caused by the human motion consists of several components (FM signals) for feature extraction we need to develop some techniques that are able to estimate the instantaneous frequency (IF) of all components. This is a challenging task since these components could be very different in magnitude and crossing in the TF plane. As a potential technique for feature extraction, we proposed the Viterbi algorithm for IF estimation applied to the TF representations. This technique is able to track signal components in the TF plane, even in the case of relatively high noise, and it is able to track the IF of crossing components.

The manuscript is organized as follows. Section 2 briefly provides an introduction to the basic mathematical description of the m-D phenomenon. Section 3 introduces the SM based approach from basic principle and demonstrates its application for extracting m-D features. The Viterbi algorithm for IF estimation is reviewed in Section 4. Results are presented in Section 5 and show that m-D features can be accurately extracted using the SM. Conclusions and recommendations for future studies are given in Section 6.

II. Basic Mathematical Description of the Micro-Doppler Phenomenon

The basic mathematical description of the m-D phenomenon induced by vibrational motions is discussed in this section. Rotation can be seen as a special case of vibration. In coherent radar, the variations in range cause a phase change in the returned signal from a target. A half-wavelength change in range can cause 360-degree phase change. It is conceivable that the vibration of a reflecting surface may be measured with the phase change. Thus, the Doppler frequency shift that represents the change of phase function with time can be used to detect vibrations or rotations of structures in a target [11]. The mathematics of the m-D effect can be derived by introducing vibration or rotation (micro-motion) to the conventional Doppler analysis. A target can be represented as a set of point scatterers, which are the primary reflecting points on the target. The point scattering model can simplify the analysis while preserving the m-D induced by micro-motions. In our case, there exists a vibrating point scatterer in a returned radar signal. The received Doppler from a target as a function of time is modeled by the following equation

$$s(t) = Ae^{[j(2\pi f_0 t + \phi(t))]}, \tag{1}$$

where A is the reflectivity of the vibrating point scatterer and f_0 is the carrier frequency of the transmitted signal. The $\phi(t)$ is the time-varying phase change of the vibrating scatterer. Assuming that the vibrating scatterer is set to a radian frequency oscillation of ω_ν, the time-varying phase is

$$\phi(t) = \beta \sin(\omega_\nu t), \tag{2}$$

where $\beta = 4\pi D_\nu/\lambda$, D_ν is amplitude of the vibration and λ is the wavelength of the transmitted signal. Substituting (2) into (1) yields $s(t) = A\exp[j(2\pi f_0 t + \beta\sin(\omega_\nu t))]$.

The phase term function in (3) is time varying, the instantaneous frequency $f_D(t)$ (IF), i.e. the m-D frequency induced by the vibration of the scatterer, may be expressed as

$$f_D(t) = \frac{1}{2\pi}\frac{d\phi}{dt}$$

$$= \frac{1}{2\pi}\beta\omega_\nu \cos(\omega_\nu t) = \frac{2}{\lambda}D_\nu\omega_\nu \cos(\omega_\nu t). \tag{3}$$

Note that the maximum m-D frequency change is $(2/\lambda)D_\nu\omega_\nu$, which is used to estimate the displacement of a vibrating scatterer. The m-D induced by vibration is a sinusoidal function of time at the vibrating frequency ω_ν. Usually, when the vibrating modulation is small, it is difficult to detect the vibration in the frequency domain. Thus, a method that is able to separate the radar return induced by the target body from that induced

by its vibrating structure might help to isolate the vibrating spectrum from other contributions. This vibration-induced m-D signature is an important feature for identifying targets of interest. An example is the human walking gait.

Modulation induced by rotating structures can also be regarded as a unique signature of a target. This m-D signature is an important feature for identifying targets of interest (e.g., helicopters, ships or aircraft with rotating antennas). When there is a rotating scatterer on a target, the phase term in (2) may be expanded as follows

$$\phi(t) = \beta \sin(\Omega t + \theta_0), \tag{4}$$

where Ω is the rotation rate and θ_0 is the rotating angle of the scatterer on the rotating structure at $t = 0$, called initial rotating angle. Therefore, the received Doppler from one rotating scatterer may be expressed by (1), which is an expansion of a vibrating structure. A detailed mathematical description of m-D modulations induced by several typical basic micro-motions is derived in [11], [18]. This description is beyond the scope of this paper.

III. S-method: Theory

In this section, we develop the SM from the basic principle. The SM based approach can be derived from the relationship between the STFT and Wigner Distribution (WD).

A. Short-Time Fourier Transform (STFT)

The most frequently used TF representation is the STFT. The idea behind the STFT is to introduce a window function $w(t)$ that truncates the analyzed signal $x(t)$ and then calculates the FT of the truncated signal. The STFT is obtained by sliding the window along the signal. The mathematical formulation of the STFT in the analog form is:

$$STFT(t,\omega) = \int_{-\infty}^{\infty} x(t+\tau)w(\tau)e^{-j\omega\tau}d\tau \tag{5}$$

where $x(t+\tau)$ is the signal shifted in time and $w(\tau)$ is a window function. The discrete form of the STFT is given:

$$STFT(n,k) = \sum_{m=-\infty}^{\infty} w(m)x(n+m)e^{-j\frac{2\pi}{N}mk}. \tag{6}$$

An energetic version of the STFT is called *spectrogram.* It is defined by:

$$SPEC(t,\omega) = |STFT(t,\omega)|^2. \tag{7}$$

The following example illustrates the STFT for different signals with different window widths. The STFT corresponds to standard FT-based radar imaging.

Example 1

Consider a Linear FM (LFM) signal $x(t)$:

$$x(t) = e^{-j160\pi t^2}. \tag{8}$$

The STFT, at the time instant $t = 0$, for different window widths T, is given in Figure 1. The Hanning window function $w(t)$ is used in this example. In this example, the STFT is dependent on the window width and non-stationary feature of the signal. To explain the above mentioned, we will use the IF, which is the first derivative of the phase. The IF of the considered signal $x(t)$ is:

$$\omega_i(t) = -320\pi t. \tag{9}$$

If considered time t interval (defined by the window function) is within the range $-\frac{T}{2} \leq t \leq \frac{T}{2}$, it follows that $\omega_i(t)$ will be in the range:

$$-\frac{320\pi T}{2} \leq \omega_i(t) \leq \frac{320\pi T}{2}. \tag{10}$$

The STFT for considered instant has the bandwidth that depends on the signal bandwidth and width of the window function in the frequency domain:

$$W_{tot} = W_{window} + W_{signal}, \tag{11}$$

where for the Hanning window has a width of that main lobe in the frequency domain equal to $W_{window} = \frac{4\pi}{T}$. The signal bandwidth is determined by (10) and it exhibits $W_{signal} = 320\pi T$, resulting in:

$$W_{tot} = \frac{4\pi}{T} + 320\pi T \tag{12}$$

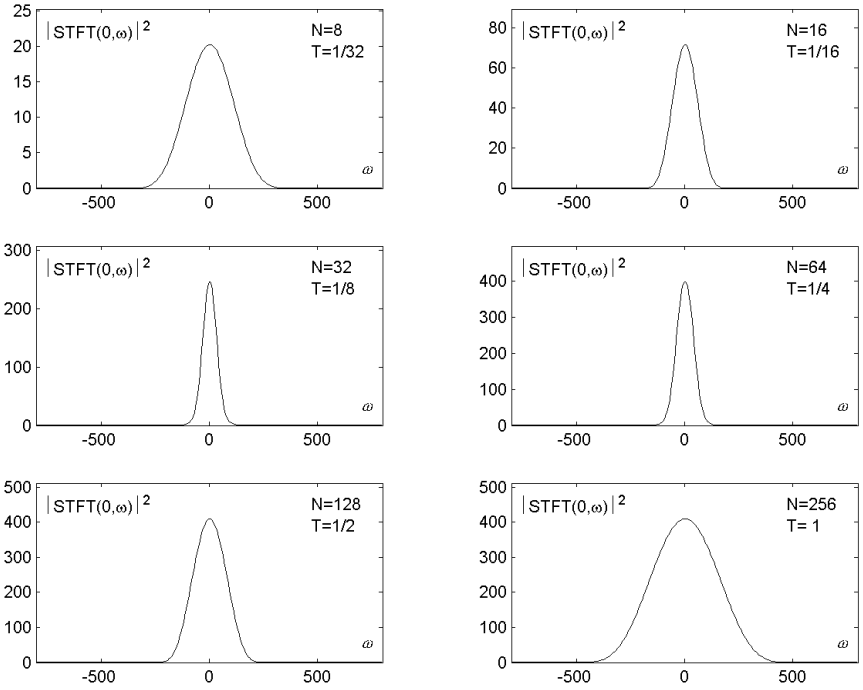

Fig. 1. The spectrogram of the linear FM signal in the time instant $t = 0$ and for various window widths.

In order to have the best possible resolution the STFT should be as narrow as possible, i.e., W_{tot} should be minimal. Then we obtain that the optimal window width follows from $\partial W_{tot}/\partial T|_{T=T_{optimal}} = 0$, as $T_{optimal} = 1/8.94$. The spectrogram calculated using this window width is close to the one depicted in Figure 1 with $T = 1/8$. The width of the spectrogram component for a small T (for example $T = 1/32$), is determined by the first term $W_{window} = 4\pi/T = 128\pi = 402$ (see Figure 1), while for the wide window (for example $T = 1$), the spectrogram width is determined by the second term $W_{signal} = 320\pi T = 320\pi = 1005$ (see Figure 1). Note that the optimal window width is highly signal dependent. When the analyzed signal is unknown, the optimal window width is also unknown. This is always the case in practice.

In addition to this, STFT does not yield sufficient time and frequency resolution simultaneously. Improving the frequency resolution by means of narrow windows results in a loss of time resolution. Short-time windows give adequate localization in time, but lead to poor frequency resolution. For improved frequency resolution, long segments of the time data must be Fourier transformed, which will then degrade the time localization.

This example clearly demonstrates that for human m-D signature analysis the STFT, i.e., spectrogram, is not a suitable tool due to the problem of resolution and concentration of components.

B. Wigner Distribution (WD)

The WD is developed as the optimal TF representation for monocomponent LFM signals. The mathematical formulation of the WD in

the analog pseudo form is [24]:

$$WD(t,\omega)=\int_{-\infty}^{\infty} w(\frac{\tau}{2})w(-\frac{\tau}{2}) \times x(t+\frac{\tau}{2})x^*(t-\frac{\tau}{2})e^{-j\omega\tau}d\tau. \quad (13)$$

In the discrete domain the WD reads:

$$WD(n,k)=\sum_{m=-\infty}^{\infty} w(m)w(-m) \times x(n+m)x^*(n-m)e^{-j\frac{4\pi}{N}mk}. \quad (14)$$

Example 2.

Consider the LFM signal given width (8). The WD of this signal is calculated in the subsequent manner:

$$WD(t,\omega)=\int_{-\infty}^{\infty} w_e(\tau)e^{-j160\pi(t+\frac{\tau}{2})^2} \times e^{j160\pi(t-\frac{\tau}{2})^2}e^{-j\omega\tau}d\tau = W_e(\omega+320\pi t)$$

where $w_e(\tau)=w(\frac{\tau}{2})w(-\frac{\tau}{2})$ and $W_e(\omega)=FT\{w_e(\tau)\}$. Thus we can conclude that the WD of the LFM signal behaves in the same way as the spectrogram of a signal with constant frequency (sinusoid). The position of the WD is determined by the IF, while its width is equal to the width of the FT of the window only. It tends to a delta function for wide windows $w(\tau)$. This is important advantage of the WD with respect to the spectrogram.

Example 3.

Consider the signal with two LFM components:

$$x(t)=x_1(t)+x_2(t) = e^{-j12\pi t^2-j10\pi t}+e^{-j12\pi t^2+j10\pi t}. \quad (15)$$

The WD of this signal is:

$$WD(t,\omega) = \int_{-\infty}^{\infty} w_e(\tau)x_1(t+\frac{\tau}{2})x_1(t-\frac{\tau}{2})^*e^{-j\omega\tau}d\tau+ \int_{-\infty}^{\infty} w_e(\tau)x_2(t+\frac{\tau}{2})x_2^*(t-\frac{\tau}{2})e^{-j\omega\tau}d\tau +2\mathrm{Re}\{\int_{-\infty}^{\infty} w_e(\tau)x_1(t+\frac{\tau}{2})x_2^*(t-\frac{\tau}{2})e^{-j\omega\tau}d\tau\}$$

where $w_e(\tau)=w(\frac{\tau}{2})w(-\frac{\tau}{2})$ and $W_e(\omega)=FT\{w_e(\tau)\}$. From the last formula it can be seen that besides the WD of auto-terms: $\int_{-\infty}^{\infty} w_e(\tau)x_1(t+\frac{\tau}{2})x_1^*(t-\frac{\tau}{2})^*e^{-j\omega\tau}d\tau$ and $\int_{-\infty}^{\infty} w_e(\tau)x_2(t+\frac{\tau}{2})x_2^*(t-\frac{\tau}{2})e^{-j\omega\tau}d\tau$, there exists a cross-term: $2\mathrm{Re}\{\int_{-\infty}^{\infty} w_e(\tau)x_1(t+\frac{\tau}{2})x_2^*(t-\frac{\tau}{2})e^{-j\omega\tau}d\tau\}$. The WD of two signal components for various window widths at the time instant $t=0$ is shown in Figure 2.

From this experiment, it can clearly be concluded that the WD is not suitable for the TF analysis of multicomponent signals. Since radar signals are inherently multicomponent and the m-D signature of humans can be represented as the sum of the FM components the WD is generally useless for their analysis. Thus, we are looking for a TF tool that is able to combine favorable properties of the STFT and WD: eliminated or reduced interferences and high concentration of signals components. In addition, from the radar signal processing perspective, it is very important that this transform can be evaluated with small calculation burden. We believe that the SM described in the next subsection is close to the trade-off between accuracy of representation and calculation efficiency.

C. S-method

In order to suppress cross-terms, a class of so-called reduced interference distributions is proposed. They are based on the Cohen definition of the quadratic TF distributions, with a kernel function being a low pass two-dimensional function. These distributions are in fact forms of the two-dimensional smoothed WD [24]. By smoothing the WD, oscillatory cross-terms are reduced. In reduced interference distributions, two important problems arise and should be stressed:

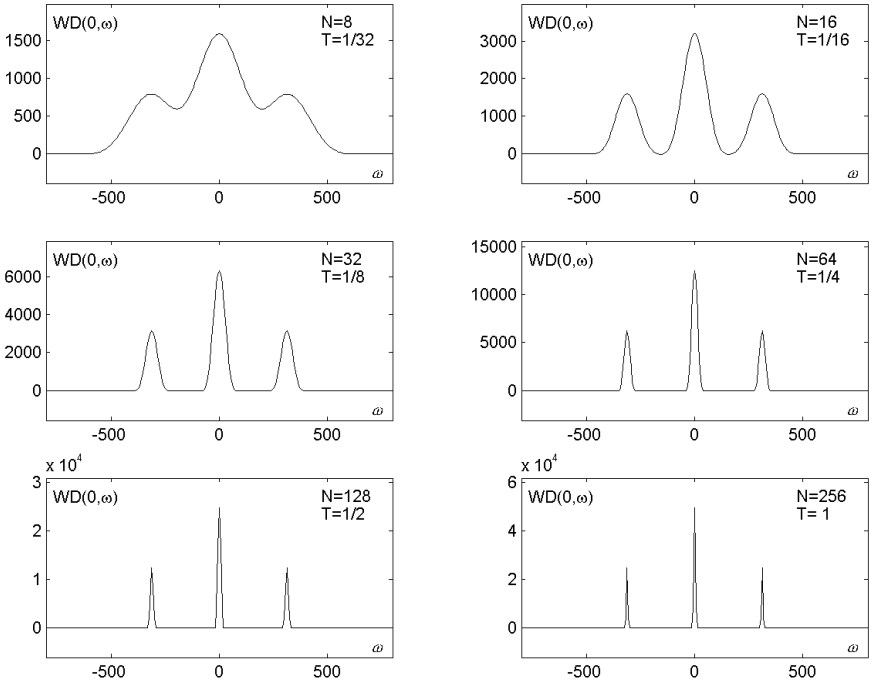

Fig. 2. The Wigner distribution of two LFM signal components $x(t)$ at the instant $t = 0$, for various window widths.

First: By smoothing the WD the auto-terms are also smoothed [25].

Second: The calculation complexity is very high, including the need for oversampling or analytic signal extension in most of the cases.

Here, we will present a computationally simple method, that can produce the same auto-terms as in the WD, but without cross-terms. It called as the SM [26]. The SM is derived from the relationship between the STFT and the WD, which reads:

$$WD(t,\omega) = \frac{1}{\pi}\int_{-\infty}^{\infty} STFT(t,\omega+\theta)STFT^*(t,\omega-\theta)d\theta. \tag{16}$$

A discrete version of the previous relation reads:

$$WD(n,k) = \sum_{i=-N/2}^{N/2} STFT(n,k+i)\times STFT^*(n,k-i)$$
$$= |STFT(n,k)|^2 \tag{17}$$
$$+2\mathrm{Re}\left\{\sum_{i=1}^{N/2} STFT(n,k+i)STFT^*(n,k-i)\right\}.$$

The mathematical formulation of the SM in the discrete form is:

$$SM(n,k) = \sum_{i=-N/2}^{N/2} P(i)STFT(n,k+i)STFT^*(n,k-i)$$

where $P(i) = 1$ for $|i| \leq L$ and $P(i) = 0$ for other values of i. The SM with L terms can be written in the form:

$$SM_L(n,k) =$$

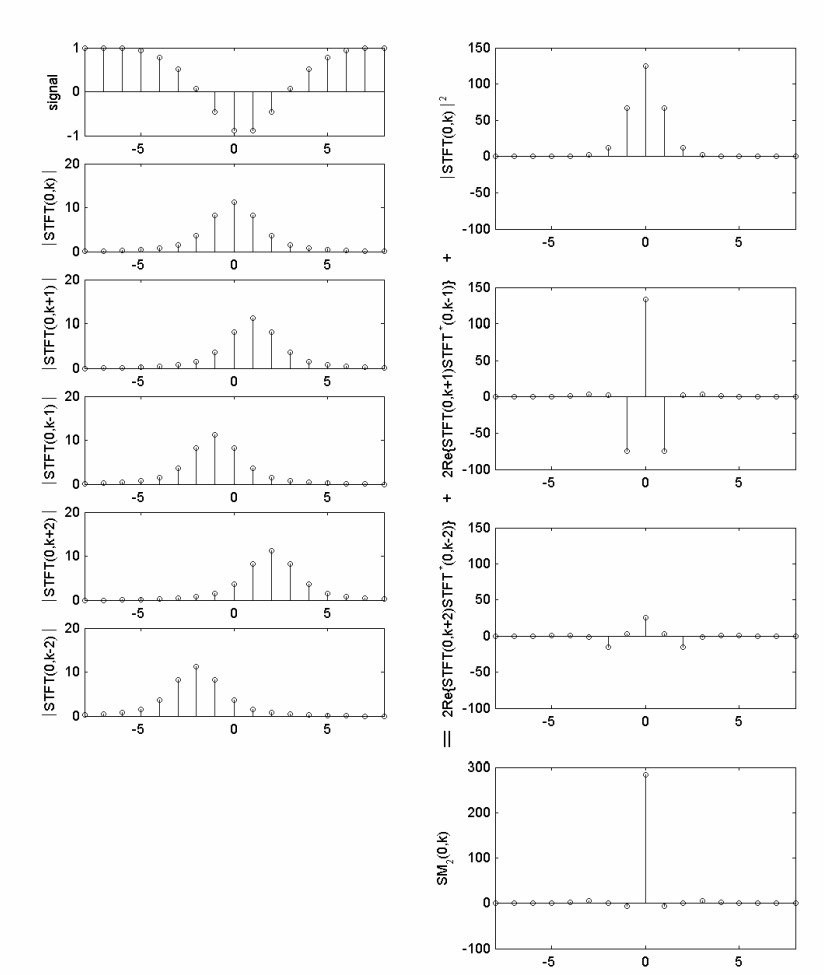

Fig. 3. The illustration for the S-method calculation for L=2: Signal (first row), STFT calculated as the signal's FFT (second row), STFT shifted for one sample left and right (third and fourth rows), STFT shifted for two samples left and right (fifth and sixth rows). The S-method is equal to the sum of the squared second row + double real part of the product of third and fourth rows + double real part of the product of fifth and sixth rows.

$$= \sum_{i=-L}^{L} STFT(n,k+i)STFT^*(n,k-i). \tag{18}$$

In particular, for $L = 0$, the SM is identical to the spectrogram

$$SM_0(n,k) = |STFT(n,k)|^2$$

$$= STFT(n,k)STFT^*(n,k),$$

while for $L = N$, the SM is identical to the WD. The illustration of the SM vector calculation for $L = 2$ is given in Figure 3. Note that SM with L terms is obtained by adding one more term to the SM with $L-1$ terms:

$$SM_L(n,k) = SM_{L-1}(n,k)$$

$$+2\mathrm{Re}\{STFT(n,k+L)STFT^*(n,k-L)\}.$$

The SM will produce the same auto terms as the WD if we take L such that $(2L+1)$ is equal to the auto terms width in the discrete domain (i.e., to the number of samples within the auto term). In practice it means fewer are needed terms, for example $L \in [3, 10]$, since most of the auto-term energy is located around its maximal value. It is shown in the next examples, that the performance of the SM is insensitive to L values in a wide range of L values. The precise mathematical proof that the the SM produces the WD of each component separately, in those regions of the TF plane where the components do not overlap, is given in [26]-[27].

Example 4

Consider three LFM signal components:

$$x(t) = x_1(t) + x_2(t)$$

$$= e^{-j8\pi t^2 - j15\pi t} + e^{-j8\pi t^2} + e^{-j8\pi t^2 + j15\pi t}. \tag{19}$$

The SM of this signal is calculated for, $N = 128$, and different L values. The S-method for all instants in the TF domain is presented in Figure 4. Figure 5 shows the SM of three components (linear and two nonlinear FM signals):

$$x(t) = e^{-j80\pi t^2 - j120\pi t + j10\sin(2\pi t) - j20\pi t}$$

$$+e^{-j160\pi t^2 + j4\cos(3\pi t) + j50\pi} + e^{j80\pi t^2 + j80\pi t}, \tag{20}$$

with fixed window width $N = 128$, and various L values. These results demonstrate that the S-method can be used to extract the m-D signatures since these signals are commonly represented as a sinusoidal FM signals (see Section 2). In addition, the technique is quite simple since the common STFT evaluator is improved with just addition of small post-processing blocks. Furthermore, the SM does not require oversampling as other bilinear representation from the Cohen class [28] and results are not as sensitive to the selection of the parameter L. All these favorable properties motivated us to apply the SM in radar signal processing and in the m-D analysis [21].

IV. M-D Feature Extraction: The Viterbi Algorithm

The m-D signatures associated to human motion are multicomponent FM signals. The extraction of the human motion features can be performed through the component separation. The analysis of components is commonly performed through the IF estimation since it contains important features of human motion such as velocity. The TF representation based IF estimators can be divided into two groups: parametric and nonparametric. In the case of parametric estimations, we can assume that m-D features are sinusoidal FM signals and for the extraction of parameters we can apply some techniques that are close to the maximum likelihood estimation or projection (Radon transform) based technique [21]. This can be applied only in the case that the number of components' parameter is relatively small or in the case when we have exact model of motion. As it can later be seen in the paper, some experimental human motions cannot be modeled as a simple sum of sinusoidal FM components. For general motion we can assume that the non-parametric IF estimation technique should be applied. The simplest non-parametric IF estimation technique is based on the position of the TF maxima:

$$\hat{k}(n) = \arg\max_k TF(n,k). \tag{21}$$

This technique is simple and well-known but it is suitable for monocomponent signals or multicomponent signals that are non-overlapping in the TF plane. In the latter case, we should perform the separation of signals from distinct regions or in the case when components significantly differ in magnitude we can perform the estimation of the dominant component. After that we can calculate the new TF representation with removed (peeled off) dominant component:

$$TF'(n,k) = \begin{cases} 0 & |k - \hat{k}(n)| \le \Delta \\ TF(n,k) & \text{elsewhere,} \end{cases} \tag{22}$$

where $(2\Delta + 1)$ is the width of the neighborhood of the dominant component removed from the TF representation. Then IF esti-

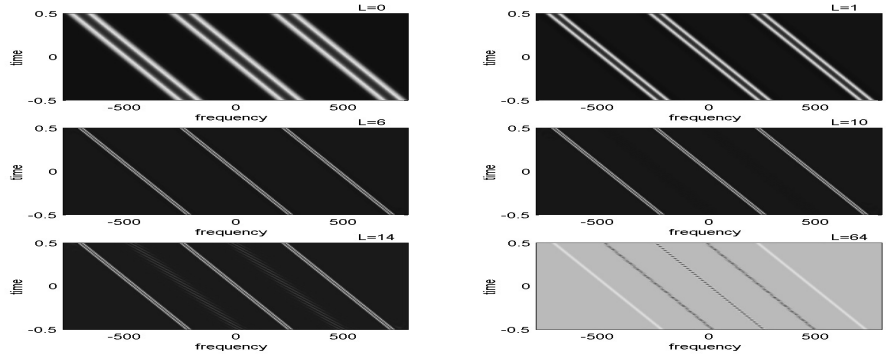

Fig. 4. SM of three LFM signal components with fixed window width $N = 128$, and different L values.

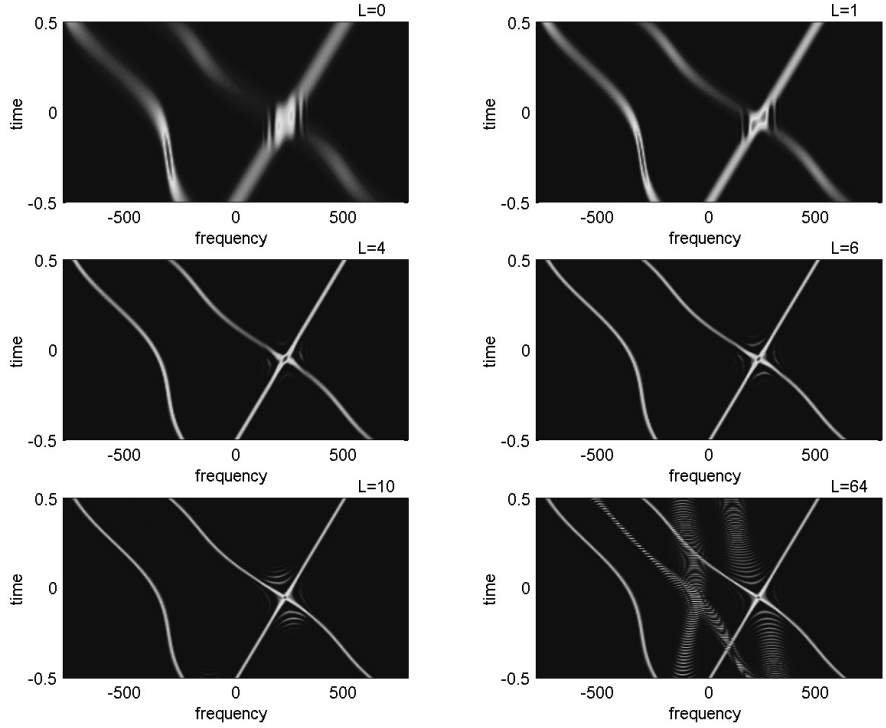

Fig. 5. The SM of three nonlinear FM signal components with fixed window width $N = 128$, and various L values.

mation of the next component can be performed by using the position of the maxima of $TF'(n,k)$. The algorithm for peeling component and IF estimation should be performed for each component. However, for multicomponent signals intersecting in the TF plane we need some more sophisticated analysis procedure. Since m-D features of the human motion have interesting components in the TF plane, both parametric techniques or simple techniques based on the position of maxima are not appropriate for its analysis and feature extraction. That is the reason for using the Viterbi algorithm for IF estimation proposed in [31] in this research.

The Viterbi algorithm is a common technique for the estimation of hidden states in the signal. The Viterbi algorithm is essentially a shortest length path algorithm that has found numerous applications in coding theory [34], image processing [35], etc. The IF estimator based on the Viterbi algorithm and TF representations is recently proposed in [31], [32]. This estimator has shown excellent accuracy for high noise environments. In development of this estimator, two assumptions are adopted:

(1) If the TF maximum at the considered instant is not at the IF point, there is a high probability that the IF is at a point having one of the largest TF values (for example second, third, but not as far as, for example, the hundredth position);

(2) The IF variation between two consecutive points is not extremely large.

Then the IF estimate can be written as the line minimizing $k(n)$, the corresponding sum of the path penalty functions $p(k(n);n_1,n_2)$:

$$\hat{\omega}(n) = \arg \min_{k(n)\in\mathbf{K}} \left[\sum_{n=n_1}^{n_2-1} g(k(n),k(n+1)) + \sum_{n=n_1}^{n_2} f(TF(n,k(n))) \right] = \arg \min_{k(n)\in\mathbf{K}} p(k(n);n_1,n_2), \quad (23)$$

where $p(k(n);n_1,n_2)$ is a sum of the penalty functions $g(x,y)$ and $f(x)$, along the line $k(n)$, from the instant n_1 to n_2. The penalty function $f(x)$ corresponds to the first assumption, while the penalty function $g(x,y)$ corresponds to the second assumption. The function $g(x,y) = g(|x-y|)$ is a nonincreasing one, with respect to the absolute difference between x and y (between the IF values in the consecutive points $x = k(n)$ and $y = k(n-1)$), while $f(x)$ is a nondecreasing function of $x = TF(n,k(n))$. In this way, the larger values of the TF are more important candidates for the position of the IF at the considered instant. For a considered n, the function $f(x)$ can be formed as follows. The TF values, $TF(n,k)$, for considered instant:

$$TF(n,k_1) \geq TF(n,k_2) \geq .... \geq TF(n,k_j) \geq ... \geq WD(n,k_M) \quad (24)$$

where $j = 1,2,...,M$, is the position within this sequence. Then, the function $f(x)$ is formed as:

$$f(TF(n,k_j)) = j-1. \quad (25)$$

For $g(x,y) = const$, the IF estimation (23) is reduced to the position of the TF maxima, i.e., the function $f(x)$ completely determines minimum of (23). In this paper, we use a linear form of $g(x,y)$, for the difference between two points greater than an assumed threshold Δ:

$$g(x,y) = \begin{cases} 0 & |x-y| \leq \Delta \\ c(|x-y|-\Delta) & |x-y| > \Delta. \end{cases} \quad (26)$$

The reasonable choice for Δ would be the maximal expected value of the IF variation between consecutive points. It means that there is no additional penalty due to this function for small IF variation (within Δ points, for two consecutive instants). In the realization we obtained good results by taking Δ which corresponds to a few neighboring points (for example, values around $\Delta = 3$). For $\Delta \to \infty$, the estimation given by (23) will reduce to the estimation based on the TF maxima. Note that this is one possible form of the penalty functions $f(x)$ and $g(x,y)$.

The reasoning for the selection of path penalty functions is described in detail in [31]. The proposed algorithm can be realized in

recursive manner with reasonable calculation complexity.

As far as we know, the proposed algorithm outperforms all other non-parametric IF estimators based on the TF representation for high noise environment. For multicomponent signals we should perform estimation component by component, peeling detected components. However, the Viterbi algorithm has the ability to connect components even in the case that some of its parts are removed. This algorithm can be expanded by the third penalty function related to the amplitude variation of the signal components. This algorithm extension is proposed in [31] where it has demonstrated its accuracy in tracking intersecting components.

V. Results

In this section we demonstrate the application and effectiveness of the S-method and Viterbi algorithm as an m-D Doppler feature extraction technique with four different types of experimental radar data obtained in different indoor and outdoor scenarios.

A. Rotation-induced micro-Doppler

A.1 Rotating corner reflector

Experimental trials were conducted to investigate and determine the m-D radar signatures of targets using an X-band radar. The target used for this experimental trial was a spinning blade with corner reflectors attached that were designed to reflect electromagnetic radiation with minimal loss. These controlled experiments can simulate the rotating types of objects generally found in an indoor environment, for example, rotating fan, and outdoor environment, for example, rotating antenna or rotors. Controlled experiments will allow us to set the desired rotation rate and then permit us to cross check and assess the results.

A picture of the target is shown in Figure 6. The blade was set up to simulate real data that might be collected from a similar target such as a rotating antenna or rotating fan or any other rotation of structures on a target. The experiment was conducted with the radar operating at 9.2 GHz. The pulse repetition frequency (PRF) was 1 kHz. The target employed in this experiment was at a range of 300 m from the radar. The SM is utilized in order to depict the m-D oscillation. The results in Figure 7a is obtained using one rotating corner reflector facing the radar. Details of the figure clearly show the sinusoidal motion of the corner reflector. The second weaker oscillation represents the reflection from the counter weight that was used to stabilize the corner reflector during operation. From the TF signature we can see that the m-D of the rotating corner reflector is a time-varying frequency spectrum. The rotation rate of the corner reflector is directly related to the time interval of the oscillations. From the additional time information, the rotation rate of the corner reflector is estimated and is about 60 rpm. Figure 7b shows the result when the blade is rotating with two corner reflectors. In this case, the rotation rate of the corner reflector is 40 rpm. Rotation rates estimated by the TF analysis agree with the actual values. These results demonstrate that the SM can be used to extract m-D features and estimate motion parameters. In a future study we will quantitatively compare the SM with other traditional m-D analysis techniques.

A.2 Rotating fan

Experimental trials were conducted to investigate and determine the m-D radar signatures of objects that could be found in indoor radar imaging. The object in these experiments is rotating fan data supplied to us by Prof. Moeness Amin, Villanova University. The rotational motion of blades in a fan imparts a periodic modulation on radar returns. The rotation-induced Doppler shifts relative to the Doppler shift of the body occupy unique locations in the frequency domain. Whenever a blade has specular reflection such as at the advancing or receding point of rotation, the particular blade transmits a short flash or periodic modulation to the radar return. The rotation rate of the blade is directly related to the time interval between these flashes. The duration of a flash is determined by the radar wavelength and by the length and rotation rate of the blades. A flash resulting from a blade with a longer length and radar with a shorter

Fig. 6. Picture of the target simulator experimental apparatus.

wavelength will have a shorter duration [9].

The fan in this experiment is rotating at a height of approximately 2 m and at a range of 3 m from the radar. The fan has 4 metallic blades. The rotation rate of the blades is known to be 1050 rpm for this data. The experiment was conducted with the radar operating at frequency of 903 Hz. The sampling frequency is 5000 Hz.

The original rotating fan data behaves like a very low pass in the frequency domain and it is quite difficult to extract any information. In order to obtain the inner micro-Doppler features, we perform down-sampling on the signal by a factor of 4 and then use a relatively narrow window of 16 samples. Figure 8a shows the S-method of the down-sampled signal with N=16 samples and L=2. When L=3 is used for the S-method, Figure 8b shows further concentration improvement. Figure 8b also exhibits that S-method can accurately describe the signal's features showing the sinusoidal behavior not just amplitude. The image in Figure 8c shows a zoomed version of the time interval between 0.13 and 0.25 seconds. This figure distinctly depicts the sinusoidal oscillation of the fan blade. From Figure 8c, the period of oscillation is 0.1/7.0 seconds. Since there are four blades, the period per blade is (0.1*4)/7. The number of rotations in one minute is given by (7*60)/(0.1*4) =1050 rpm/blade, which is in agreement with the actual value known to be 1050 rpm.

B. Vibration-induced micro-Doppler

B.1 Human walking

Gait recognition by radar focuses on the gait cycle formed by the movements of a person's various body parts over time. Radar echoes contain rich information about the various parts of the moving body. Various body parts have different shifts since they are moving with various velocities. For example, a walking man with swinging arms may induce frequency modulation of the returned signal and generate side-bands about the body Doppler. There are often multiple physical movements taking place simultaneously and it is the interaction of these that produces the

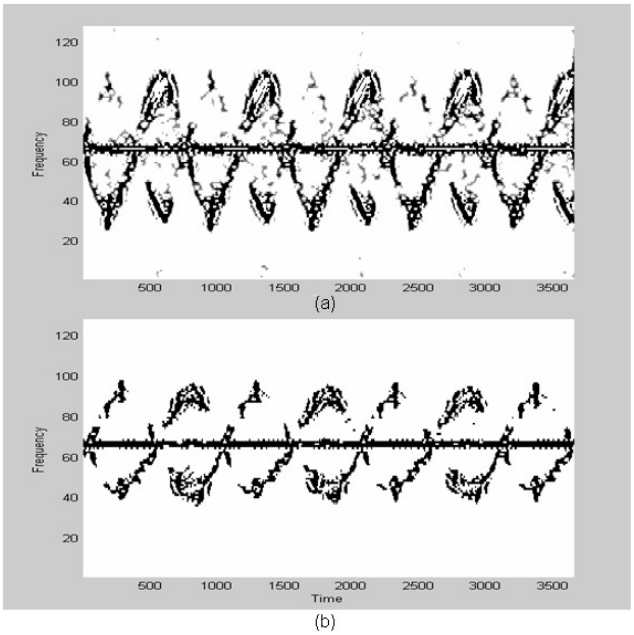

Fig. 7. S-method of experimental data: (a) m-D effects from one rotating corner reflectors facing the radar; (b) m-D effects from two rotating corner reflectors facing the radar. Note that 3650 time samples correspond to 5.2 seconds of data.

particular characteristics of a "gait". Radar experiments were conducted and the proposed SM based approach is used to analyze the Doppler shift of the body and the m-D signature of the swinging arms and to estimate gait parameters such as swinging rate.

In this experiment we considered the human data. The main part of a human body causes the strongest component as it can be seen from the SM of the considered signal Figure 9a. For the analysis of other components, caused by swinging arms and moving legs, we need to remove the main body component. The classical IF estimator based on the position of the TF representation maxima is used in the first stage of the algorithm [30]:

$$\hat{k}(n) = \arg\max_{k} SM(n,k). \tag{27}$$

This IF estimate corresponds to the strongest component, in this case the main body component. Figure 9b depicts that the IF estimation is superposed onto the same TFR graph. Then, classical peeling techniques can be employed to remove the main body component from the rest of the TF representation:

$$SM'(n,k) = \begin{cases} 0 & |k-\hat{k}(n)| \leq \Delta \\ SM(n,k) & \text{elsewhere,} \end{cases} \tag{28}$$

where $2\Delta+1$ is number of samples around the IF of the main component removed from the SM. The TF representation with 'the peeled-off' main body component is depicted in Figure 9c. Now other weaker components can be clearly seen. These components correspond to the moving legs and arms. Components with smaller amplitude correspond to the moving arms while components with larger amplitude (larger frequency variations) correspond to the moving of legs. It can be easily noticed that the moving leg produces sinusoidal FM signal

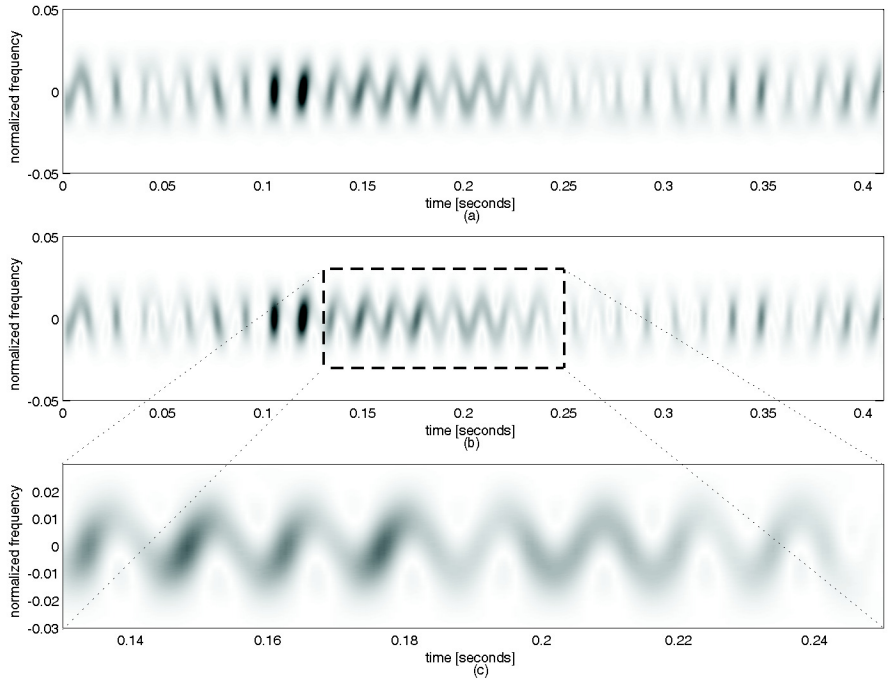

Fig. 8. Time-frequency representations of fan data: (a) SM with L=2; (b) SM with L=3; and (c) Zoomed version of (b).

during the relative motion of the leg but in the next step this component has slowly a varying component and we have that the second leg produces 'semi-period' of the sinusoidally FM signal. This clearly shows that in this case it is not possible to use the radon transform or parametric estimator for extraction of the component.

In this case we cannot claim that one component is dominant over others since their magnitudes are similar and they are crossing in the TF plane. The algorithm based on the position of the TF representation maxima would give a line that is a combination of the IFs of different components. Then a more sophisticated algorithm for the IF estimation and segmentation of these components is required. A simple scheme such as (27) cannot produce accurate results for separation of these components. Here, the Viterbi algorithm for the IF estimation is used [31]. This algorithm is able to track the component in the TF plane that are intersected even for relatively high noise environment. Figure 9d depicts the IF estimation of the next component associated with the leg motion based on the Viterbi algorithm. It can be seen that the component is recognized in a proper manner except for the small part around the intersection of this component, which is caused by both the second leg component and the main body motion component. After peeling of this component, the next component can be determined in a similar manner. However, complicated signatures such as those produced by human motion require a very detailed analysis of the Viterbi algorithm parameters with possible alternative techniques for selecting the path penalty functions. This topic remains for future research.

B.2 Human walking in a high noise environment

In order to demonstrate the effectiveness of the Viterbi algorithm in a high noise envi-

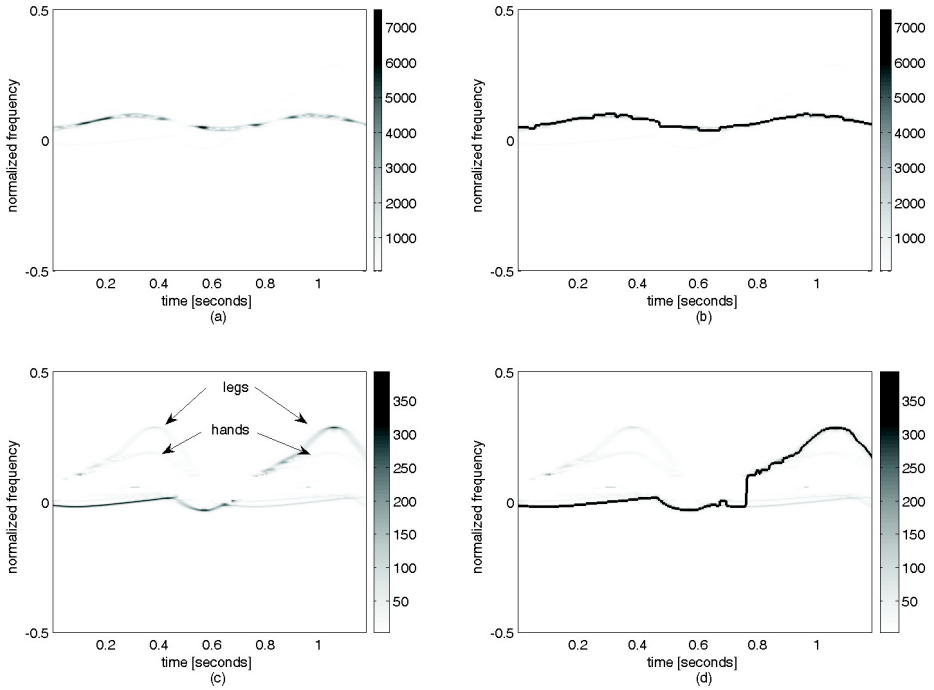

Fig. 9. Time-frequency representations and IF estimation for human data: (a) Time-frequency representation of m-D of a walking man signal; (b) Instantaneous frequency estimation of the main body component; (c) Time-frequency representation of m-D of a walking man signal, after removing the main body component; (d) Instantaneous frequency estimation of the weak component by using the Viterbi algorithm.

ronment, an experimental human data is analyzed. The human data used in this experiment was collected in a relatively high noise real environment using the EARS experimental array Rrdar system (EARS) employing a stepped frequency radar waveform [21,23]. In this experiment, a human is marching on the spot towards the radar swinging one arm. The distance of the human from the radar is about 300 m. The experiment was conducted with the radar operating at frequencies of 8.9 to 9.4 GHz, providing a 500 MHz bandwidth. The frequency step size was 10 MHz and a pulse repetition frequency (PRF) of 1 kHz was used. Thus, it required 50 ms to generate a single high-range resolution (HRR) profile (i.e. an effective HRR PRF of 20 Hz). The integration time for each data set was 60 seconds.

Figure 10a shows the image using the S-method. No feature information can be extracted from this figure. Figure 10b shows the same image using the S-method but the high frequency content is filtered. The IF estimation based on the position of the maxima is depicted in Figure 10c by the solid line, while the output of the Viterbi algorithm is given by the dash line. The arrows represent the position of the obvious mistakes in the case of the algorithm based on the position of the SM maximum. These mistakes are caused by the small amplitude of the TF representation in the considered interval. In Figure 10d we added artificial noise in order to describe the situation when recordings are corrupted by high amounts of noise. The SNR ratio between recordings and added noise in this case is just 1.5 dB. In this case the algorithm based on the position of the maximum (Figure 10e, solid line) is useless since it produces numerous mistakes. However the VA based al-

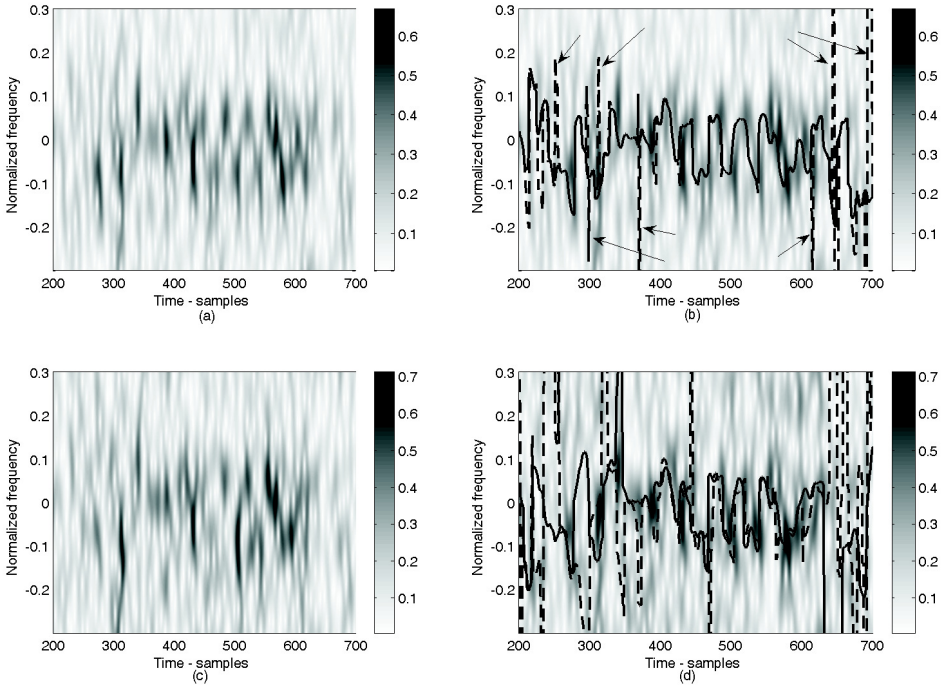

Fig. 10. Time-frequency representations and IF estimation for human experimental data in noisy environment: (a) SM with no added noise; (b) SM with IF estimation (solid line position of the maxima, dash line Viterbi algorithm, arrows obvious errors in the algorithm with position of maximum); (c) SM method with signal corrupted by noise; (d) SM with IF estimation for noisy signal (solid line position of the maxima, dash line Viterbi algorithm).

gorithm remains very accurate at least in the central part of the recording (between samples 300 and 600) where the signature of the useful signal is relatively large. These results suggest that the VA algorithm and SM are promising in this application even under non-ideal conditions. It should be noted that the EARS is not built for micro-Doppler type experiments and does not possess the coherency necessary to extract the full range of micro-motions. A highly coherent (low-phase noise) radar is desirable to extract human m-D features.

VI. Conclusion

Micro-Doppler features have great potential for use in automatic target recognition algorithms. Although the potential benefit of using a micro-Doppler in recognition algorithms is high, relatively little experimental m-D data exists. This paper involves data collection and analysis of indoor and outdoor m-D radar signatures. In order to extract and enhance the m-D features, the S-method based approach and the Viterbi algorithm are proposed to analyze and resolve radar m-D signatures of targets. The S-method is computationally simple, requiring only slight modifications to the existing Fourier transform-based algorithm. It is shown that the S-method based approach provides an effective method of achieving improved resolution, highly concentrated and readable representation without the auto-term distortion and cross-term artifacts. This method in conjunction with the Viterbi algorithm are suitable for m-D data where multiple scatterers are present, and noise and artifact reduction are essential for target identification applications. The effec-

tiveness of the S-method in conjunction with Viterbi algorithm in extracting m-D features is demonstrated through the application to experimental indoor rotating fan data and outdoor human data. We hope that this new approach will also find a wide range of uses and will emerge as a powerful tool for time-varying spectral analysis.

VII. Acknowledgments

We would like to thanks Prof. Moeness Amin, Villanova University for supplying to us the indoor rotating fan data. We would also like to thank Dr. V. Chen of Naval Research Laboratory, USA, for supplying with us the human data. We would like to thank E. Riseborough, D. Lamothe, and I. Grant for the support during experimental trials and data collection.

References

[1] C. P. Lai, Q. Ruan, and R. M. Narayanan, "Hilbert-Huang Transform (HHT) processing of through-wall noise radar data for human activity characterization," *Proc. IEEE SAFE 2007 Workshop on Signal Processing Applications for Public Security and Forensics*, Washington, DC, March 2007.

[2] F. Ahmad, M. G. Amin, and P. D. Zemany, "Performance analysis of dual-frequency CW radars for motion detection and ranging in urban sensing applications," *Proc. SPIE Symposium on Defense and Security, Radar Sensor Technology XI Conference*, vol. 6547, Orlando, FL, April 2007.

[3] P. Setlur, F. Ahmad, M. G. Amin, and P. D. Zemany, "Experiments on through-the-wall motion Detection and ranging," *Proc. SPIE Symposium on Defense and Security, Sensors, and Command, Control, Communications, and Intelligence (C3I) Technologies for Homeland Security and Homeland Defense VI Conference*, vol. 6538, Orlando, FL, April 2007.

[4] P. van Dorp, P., and F. C. A. Groen, "Human walking estimation with radar", *IEE Proc-Radar Sonar Navig.,* Vol. 150, No. 5, 2003.

[5] J. L. Geisheimer, E. F. Greneker, and W. S. Marshall, "A high-resolution Doppler model of human gait", *Georgia Tech. Research Institute*, 7220 Richardson Rd., Smyrna, GA 30080.

[6] J. J. Little, and J. E. Boyd, "Recognizing people by their gait: the shape of motion", *Journal of Computer Vision Research,* vol. 1, no. 2m 1998.

[7] S. A. Niyogi, and E. H. Adelson, "Analyzing and recognizing walking figures in XYT", *IEEE Proceedings on Computer Vision and Pattern Recognition,* pp. 469-474, 1994.

[8] A. M. Sabatini, and V. Colla, "A method for sonar based recognition of walking people", *Robotics and Autonomous Systems,* Vol. 24, pp. 117-126, 1998.

[9] R. F. Weir, and D. S. Childress, "A new method of characterizing gait using a potable, real-time, ultrasound ranging device", *Proceedings of the 19th International Conferenc of the IEEE Engineering in Medicine and Biology Society*, pp. 1810-1812, 1997.

[10] S. Sundar et al, "Doppler-based detection and tracking of humans in indoor environments," Special Issue on Indoor Radar Imaging, *Journal of Franklin Institute*, July 2008.

[11] V. C. Chen, and H. Ling, *Time-frequency transform for radar imaging and signal analysis*, *Artech House,* Boston, 2002.

[12] V. C. Chen, "Analysis of radar micro-Doppler signature with time-frequency transform", *Proc. Tenth IEEE Workshop on Statistical Signal and Array Processing,* pp. 463-466, 2000.

[13] T. Sparr, and B. Krane, "Micro-Doppler analysis of vibrating targets in SAR", *IEE Proc-Radar Sonar Navig.,* Vol. 150, No. 4, pp. 277-283, 2003.

[14] T. Thayaparan, S. Abrol, E. Riseborough, L. Stanković, D. Lamothe, and G. Duff. (2007), "Analysis of Radar Micro-Doppler Signatures From Experimental Helicopter and Human Data," *IEE Proceedings Radar Sonar Navig.,* 1, (4), pp. 288-299.

[15] T. Thayaparan, S. Abrol, V. C. Chen, and E. Riseborough: "Analysis of Micro-Doppler radar signatures from experimental helicopter and human data", *NATO SET-80 symposium*, Oslo, Norway, Oct. 2004.

[16] J. Misiurewicz, K. Kulpa, and Z. Czekala: "Analysis of recorded helicopter echo", *Proceedings of IEE Radar 98,* pp. 449-453.

[17] V. C. Chen, F. Li, S.-S. Ho, and H. Wechsler: "Analysis of micro-Doppler signatures," *IEE Proc. Radar, Sonar, Navig.*, Vol. 150, No. 4, Aug. 2003, pp. 271-276.

[18] V. C. Chen, F. Li, S.-S. Ho, and H. Wechsler, "Micro-Doppler effect in radar: phenomenon, model, and simulation study", Vol. 42, No. 1, pp. 2-21, *IEEE Trans. on Aerospace and Electronis Systems,*, 2006.

[19] J. Li, and H. Ling: "Application of adaptive chirplet representation for ISAR feature extraction from targets with rotating parts", *IEE Proc. Radar, Sonar, Navig.*, Vol.150, No.4, August 2003, pp.284-291.

[20] T. Thayaparan, "Micro-Doppler analysis of the rotation antenna in airborne SAR image collected by the APY-6 radar," *IRS 2005*, Berlin, Germany, Sept. 2005.

[21] L. Stanković, T. Thayaparan, and I. Djurović, "Separation of target rigid body and micro-Doppler effects in ISAR imaging", *IEEE Trans. on AES,* Vol. 41, No. 4. pp. 1496-1506, 2006.

[22] W. J. Williams, and E. J. Zalubas: "Invariant classification of time-frequency representations: Applications to Doppler radar target identification," in *Proc. of DSTO/DOD Workshop*, Adelaide, Austr. 1997.

[23] P. Setlur, M. Amin, and T. Thayaparan: "Micro-Doppler signal estimation for vibrating and rotating targets," in *Proc. of ISSPA 2005*, Sydney, Austr. 2005, pp. 639-642.

[24] L. Cohen, *Time-frequency analysis*, Prentice-Hall Inc., New York, USA.

[25] L. Stanković, "The auto-term representation by the reduced interference distributions: The procedure for a kernel design", *IEEE Trans.on Signal Processing*, Vol. 44, No. 6, pp. 1557-1564, 1996.

[26] L. Stanković, "A method for time-frequency analysis," *IEEE Trans. Signal Process.*, Vol. 42, pp. 225-229, 1994.

[27] L. Stanković, I. Djurović: "A note on 'An overview of aliasing errors in discrete-time formulations of time-frequency representations' ", *IEEE Trans. on Signal Processing*, vol.49, no.1, Jan.2001, pp.257-259.

[28] L. Stanković, "An analysis of some time-frequency and time-scale distribution," *Annales des Telecomm.*, Vol. 49, No.9-10, pp. 505-517, 1994.

[29] T. Thayaparan, G. Lampropoulos, S. K. Wong, and E. Riseborough, "Application of adaptive joint time-frequency algorithm for focusing distorted ISAR images from simulated and measured radar data," *IEE Proc. Radar, Sonar Navig.,* Vol. 150, No. 4, pp. 213-220, 2003.

[30] B. Boashash, "Estimating and interpreting the instantaneous frequency of a signal - Part I," *Proc. IEEE*, Vol. 80, No.4, Apr. 1992, pp. 521-538.

[31] I. Djurović, and LJ. Stanković: "An algorithm for the Wigner distribution based instantaneous frequency estimation in a high noise environment", *Signal Processing*, Vol. 84, No. 3, Mar. 2004, pp. 631-643.

[32] LJ. Stanković, I. Djurović, A. Ohsumi, and H. Ijima: "Instantaneous frequency estimation by using Wigner distribution and Viterbi algorithm", in *Proc. of ICASSP 2003*, Hong Kong, China, Apr. 2003, Vol. VI, pp. 121-124.

[33] C. Cornu, I. Djurović, C. Ioana, A. Quinquis, and LJ. Stanković, "Time-frequency detection using Gabor filter banks and Viterbi based grouping algorithm," in *Proc. of IEEE ICASSP'2005*, Philadelphija, USA, Mar. 2005, USA, Mar. 2005, Vol. 4, pp.497-500.

[34] G. D. Forney, "The Viterbi algorithm," *Proc. IEEE*, Vol.61, No.3, Mar. 1973, pp. 268-278.

[35] A. Martell: "Edge detection using heuristic search methods," *Computer Graphics and Image Processing*, Vol. 1, No. 2, Aug. 1982, pp. 169-182.